High-pressure STM studies of oxidation catalysis
Bobaru, Ş.C.

Chapter 3

CO oxidation over palladium surfaces

In this Chapter we describe and interpret Scanning Tunneling Microscopy and Mass Spectrometry experiments on CO oxidation at ambient pressure and elevated temperatures over three palladium surfaces: Pd(100) ,its vicinal surface Pd(1.1.17) and Pd(553). We show that all three surfaces can be oxidized under sufficiently oxygen-rich conditions, which is accompanied by a change in reaction kinetics. On two of these three surfaces we observe reaction oscillations.

3.1 Motivation

As a catalyst palladium is known to be highly effective for various oxidation reactions such as the complete oxidation of hydrocarbons in automotive exhaust gas and methane combustion in advanced, low NO_x gas turbines. Palladium-based alloys are actively investigated for applications in fuel technology. Palladium's ability to absorb and re-emit hydrogen depending on temperature and pressure conditions makes it an efficient material to filter hydrogen. Palladium is also a critical catalyst in the manufacture of polyester and in the removal of a number of toxic and carcinogenic substances from ground water [1-7]. Other important reactions for palladium catalysts are the hydrogenation of olefins and aromatic nitro compounds. Self-sustained oscillations in the reaction rate have been observed during CO oxidation over palladium crystals. Since the understanding of the mechanism behind the self-sustained oscillations has great importance in physics, chemistry, biology and technology, palladium is also a popular model catalyst in fundamental catalysis research [8-10]. In addition, palladium is used to make springs for watches, surgical instruments, electrical contacts and dental fillings and crowns. And palladium is also compatible with human tissue and it is used, in a radioactive form, in the medical industry for the treatment of cancer [1].

3.2 Relation between the efficiency and the crystal structure of a palladium catalyst: a literature overview

Experimental studies have revealed that the catalytic combustion over Pd catalyst is a structure sensitive reaction (the rate depends on the detailed geometrical structure of the surface atoms of the catalyst) [11-13]. Structure sensitivity usually manifests itself as a dependence of the rate per surface atom on the average size of the catalyst particle. For example, Henry et al.,

who showed that the average CO chemisorption energy increases strongly with decreasing particle size, have demonstrated the structure sensitivity for CO adsorption on small Pd particles [14]. The high efficiency of palladium has been ascribed to its ability to dissociate oxygen molecules by forming a surface oxide [15]. Also the oscillations in the CO and CH_4 oxidation rates [16-20] and the extreme sensitivity of the CH_4 oxidation rate to catalyst history [3-5,20] have been attributed to a transition between the metallic and the oxidic state. In the light of these observations it is no wonder that numerous studies have been initiated in order to characterize the oxidation and reduction mechanism of Pd surfaces on the atomic scale using a variety of surface science techniques. For example, E.H. Voogt and co-workers have studied the interaction of oxygen with Pd(111) and with a palladium foil by use of ellipsometry, LEED, AES and XPS in the temperature range of 300 to 770 K and at pressures up to 1 Pa [21]. They have reported the formation of a surface oxide at higher temperatures (T>470 K) and pressures (P>10^{-4} Pa), ascribed to a square lattice with a=7.5±0.5Å and domains in six orientations. It was not possible to match this structure with a simple overlayer structure on the (111) plane or with an unreconstructed crystal plane of PdO. G. Zeng and E.I Altman have examined the oxidation of Pd(111) [22] and Pd(100) [23] by means of TPD, LEED and in-situ, variable-temperature STM. The oxidation of Pd(111) was observed to proceed in three stages, involving four distinct oxygen phases, all stages showing a strong dependence on the oxygen coverage. In the third stage corresponding to oxygen coverages higher than 2.2 ML the formation of a bulk PdO oxide was observed. The same was found for Pd(100) with the difference that bulk oxidation proceeded on this surface through four stages involving up to five surface phases. On both surfaces, bulk PdO formation is accompanied by surface roughening. The more open Pd(100) surface has shown a higher reactivity towards O_2. Density Functional Theory (DFT) calculations have suggested that for Pd, thin surface oxides can be stable at atmospheric pressure, in oxygen-rich flow [24]. In summary there is enough experimental and theoretical evidence for the formation of palladium oxides under certain reaction conditions. In spite of this large amount of information there is no consensus concerning the role played by these oxides in the chemical reactions. In the next section of this chapter we will provide direct experimental proof that the surface palladium oxides are intermediate products of the reaction, which act as active catalysts for the oxidation of CO at atmospheric pressure.

3.3 Electronic and structural information about Pd

Before showing the experimental results we mention a few bulk properties of our model catalyst material. Palladium is one of the late 4d transition metals. It has 46 electrons per atom and an almost complete 4f shell. The

equilibrium crystal structure of Pd is a face-centered cubic Bravais lattice, with one atom in the primitive unit cell. The lattice constant at room temperature is a_{exp}=3.89 Å and the nearest-neighbour distance between Pd atoms is 2.75 Å. The Pd(100) surface has a square symmetry, Fig.3.1. The step height is 1.96 Å. The Pd(1.1.17) has (100) terraces of 8.5 atoms wide separated by (111) monoatomic steps (not shown in Fig.3.1). The Pd(553) surface is vicinal to the (111) low-index surface and consist of (111) terraces with a width of 5 atoms (10.3 Å) separated by monoatomic, (111)-type steps.
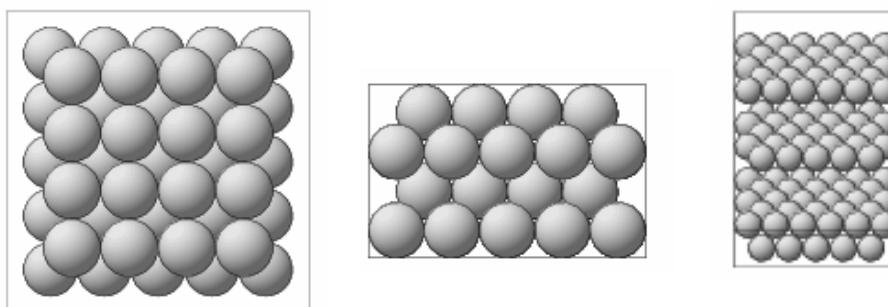
Figure 3.1: *The profile and side view of the (100) surface of a palladium crystal, and the Pd(553) surface represented as a ball model.*

3.4 Experimental

The Pd single crystal was cut by spark erosion polished mechanically to within 0.1° from the (100) orientation [25]. After introduction into the UHV chamber, the sample was cleaned by repeated cycles of 600 eV Ar-ion bombardment at 300 K, followed by annealing at 900 K in 10^{-6} mbar oxygen, and by a short flash to ~1100K in UHV until a clear LEED pattern was obtained.

3.5 Results and discussion

Figure 3.2 displays the oscillatory behaviour of the CO+O_2 reaction over Pd(100) at a constant total pressure of 1.25 bar and a temperature of 408 K. In figure 3.2 a the partial pressures of the reactant gases CO and O_2 and the reaction product CO_2 are depicted. The experiment started at t = 0 s in a CO-rich flow. At t = 188 s we switched to an O_2-rich flow (indicated by the dashed line). In response, the reaction rate, which can be read off from the partial pressure of CO_2, initially increased, passed through a maximum at t = 610 s and then decreased as the CO pressure was slowly lowered further. This behaviour is fully consistent with Langmuir-Hinshelwood kinetics (Chapter 2). At t = 3615 s there was a sudden step up in the CO_2

pressure (indicated by arrow number 1) and spontaneous oscillations followed. Coinciding with the upward step in the reaction rate we see a downward step in the CO partial pressure. We attribute the sudden increase in the reaction rate to a transition from a metallic surface with low catalytic activity to a surface oxide with higher catalytic activity [26-28]. In Chapter 2 of this thesis we have already mentioned that the CO oxidation over an oxide does not proceed via the "classic" Langmuir-Hinshelwood mechanism. The reaction occurs via the Mars van Krevelen mechanism, which requires the presence of a surface oxide and involves reactions between CO molecules from the gas phase and oxygen atoms from the surface oxide. Later in this section we provide further evidence for this scenario by use of STM images simultaneously recorded with the reaction kinetics. The oscillations in Fig.3.2 (a) have a block-wave character. At the beginning of the oscillation the times spent at the upper and lower reactivities were comparable (110 s and 90 s, respectively). At later times, i.e. for lower P_{CO}, the surface spent significantly less time in the metallic phase (31 s) while the time spent in the oxide phase decreased only slightly (72 s). This made the shape of the oscillations gradually changes from the initial square wave pattern to a series of (negative) peaks. While the CO partial pressure dropped, the CO_2 production rate in the metallic phase remained more or less constant, while the rate in the oxidic phase decreased, until at ~6500 s the difference between the two could no longer be observed. At t = 6909 s we have manually added a small amount of CO in the reactor. Simultaneously with the resulting increase in CO signal the reaction rate briefly dropped (marked by arrow 2 in the Fig.3.2 (a)) and immediately increased again. At this point, we have no explanation for this temporary dip in the reaction rate. At t = 8283 s (indicated by arrow number 3) the reaction rate again spontaneously increased stepwise, simultaneous with a decrease of the CO pressure and the catalytic system started again to spontaneously oscillate. This shows that the surface switched to the oxide phase and that immediately before 8283 s it must have been in the metallic state. The new series of oscillations evolved in time almost identically to the first oscillation series. At t = 10854 s we have switched to a CO rich flow. After a tiny, initial dip, the reaction rate passed through a significant maximum. Although we again have no explanation for the small dip, the maximum in the CO_2 production is easily recognized as Langmuir-Hinshelwood behaviour, starting with a low production on a surface dominated by adsorbed oxygen atoms (*not* an oxide), passing through a maximum-rate when the coverages of the two reacting species are equal ($\theta_{CO} = \theta_O = 0.5$), to end up at a dramatically decreased rate when the partial pressure of CO is high enough to make CO poison the surface. When we again increased the O_2 partial pressure at t = 17673 s, the reaction rate initially increased, then passed through a maximum, after which it decreased again. This is the same sequence of Langmuir-Hinshelwood kinetics in reversed order. After this we

observed a sequence of oscillations, starting at t = 20953 s, that was very similar to the first two series of oscillations. We now have a more detailed look at the first series of oscillations, which we plot in Fig.3.2 (b) as the CO_2 pressure (P_{CO_2}) as a function of CO pressure (P_{CO}). All data in this plot fall on two reaction branches, reflecting the bistability of the system. These two branches have been identified before for Pt(110) [26]. The lower branch corresponds to the Langmuir-Hinshelwood reaction on the metallic surface (R_{metal}), the higher branch to the Mars-van-Krevelen reaction on the oxide surface (R_{oxide}). What is different from the case of Pt(110) is that the present catalytic system of CO oxidation on Pd(100) is unstable and the system oscillates between the two states of the surface. We have observed that the reaction rate on the oxide branch is proportional to P_{CO} while the reaction rate on the metallic surface depends on both P_{CO} and P_{O_2}. In Fig.3.2 © we have the same type plot for the second oscillation series, to illustrate that this series is almost identical to the first series of oscillations. In the sequence of Fig.3.2 (a) the surface has been brought into and taken out of oscillation three times. The ratio $P_{CO}/\sqrt{P_{O_2}}$ at which the metal surface switched to the oxide and started to oscillate amounted to 0.040 √bar, 0.039 √bar and respectively 0.037 √bar. From the small but statistically significant reduction in this ratio we see that after every series of oxidation-reduction oscillations, the surface oxidizes at a somewhat lower $P_{CO}/\sqrt{P_{O_2}}$ ratio. Combined with our observation that the oxidation-reduction cycles slowly makes the surface more and more rough (see below), this suggests that the $P_{CO}/\sqrt{P_{O_2}}$ ratio at which the surface oxidizes depends on the surface roughness and is thus sensitive to the 'history' of the model catalyst.

All our experiments concerning the oscillatory oxidation of CO over Pd(100) exhibited hysteresis in the CO_2 production rate (upon variation of P_{CO}) with a counter-clockwise orientation in the P_{CO_2}-versus-P_{CO} plot. In other words the oxide was formed on the Pd(100) surface at a higher P_{CO} value than that at which it was later reacted away. This observation is consistent with previous experimental studies performed by other researchers in the field of oscillatory CO oxidation on palladium surfaces, which also indicate the requirement of counter-clockwise hysteresis for the occurrence of oscillations [9, 16].

The upper part of Figure 3.3 shows a series of STM images, which were recorded simultaneously with the self-sustained oscillation plotted in the lower panel. Image A has been acquired immediately before the first oscillation. It shows the metallic surface with (rounded) square adatom islands, reflecting the symmetry of the (100) plane. The measured height of the adatom islands is equal to the monoatomic step height of Pd(100) of 1.96 Å. Image B was acquired at the same position, immediately after image A. Despite the low resolution one can recognize a noticeable difference in the morphology of the surface compared to image A. The adatoms islands have

disappeared or have been replaced by a high density of cluster structures. Image B was recorded immediately after the step up in the reaction rate.
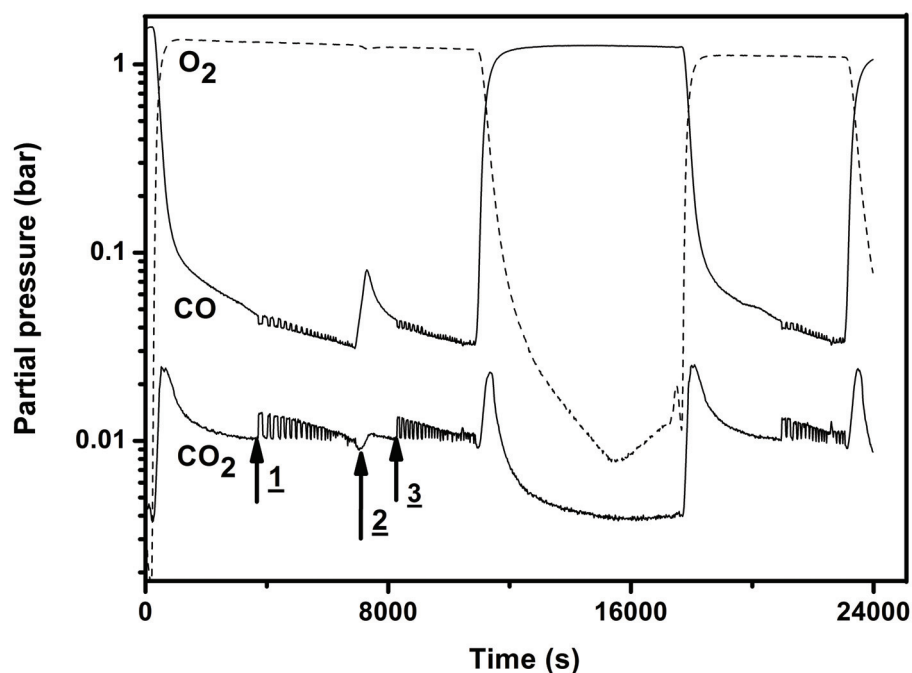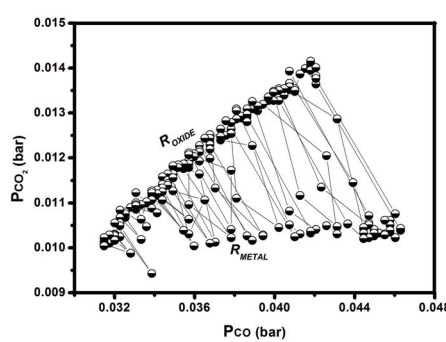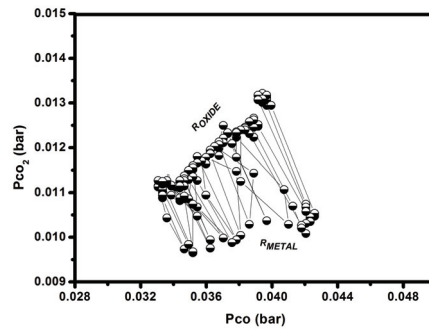
Figure 3.2: *(a) Partial pressures of CO, O_2 and CO_2 on Pd(100) at T = 408 K and P_{tot} = 1.25 bar. The CO and O_2 pressures were regulated (upstream), while the CO_2 reflects the catalytic conversion rate. The first and second series of oscillations in these measurements have been re-plotted in panels (b) and (c) respectively as P_{CO_2} against P_{CO}.*

The sudden increase in the reaction rate correlated with the change in the surface structure in an oxygen-rich environment suggests that the surface switched from a metal to an oxide with higher reactivity towards CO oxidation, similar to what has been found previously on Pt(110) [26]. The

changes in the surface structure associated with the variations in reactivity are better illustrated by images C and D. They were acquired during the third and the fourth periods of the first series of oscillations. In both images, the surface spontaneously switched between a structure with monolayer deep protrusions and depressions with square symmetry (lower part of images C and D), corresponding to the metal, to structures with a rougher appearance and with non-integer height differences, corresponding to the oxide (upper part of the images). Images illustrate that the self-sustained oscillations are spontaneous metal-oxide phase transitions.
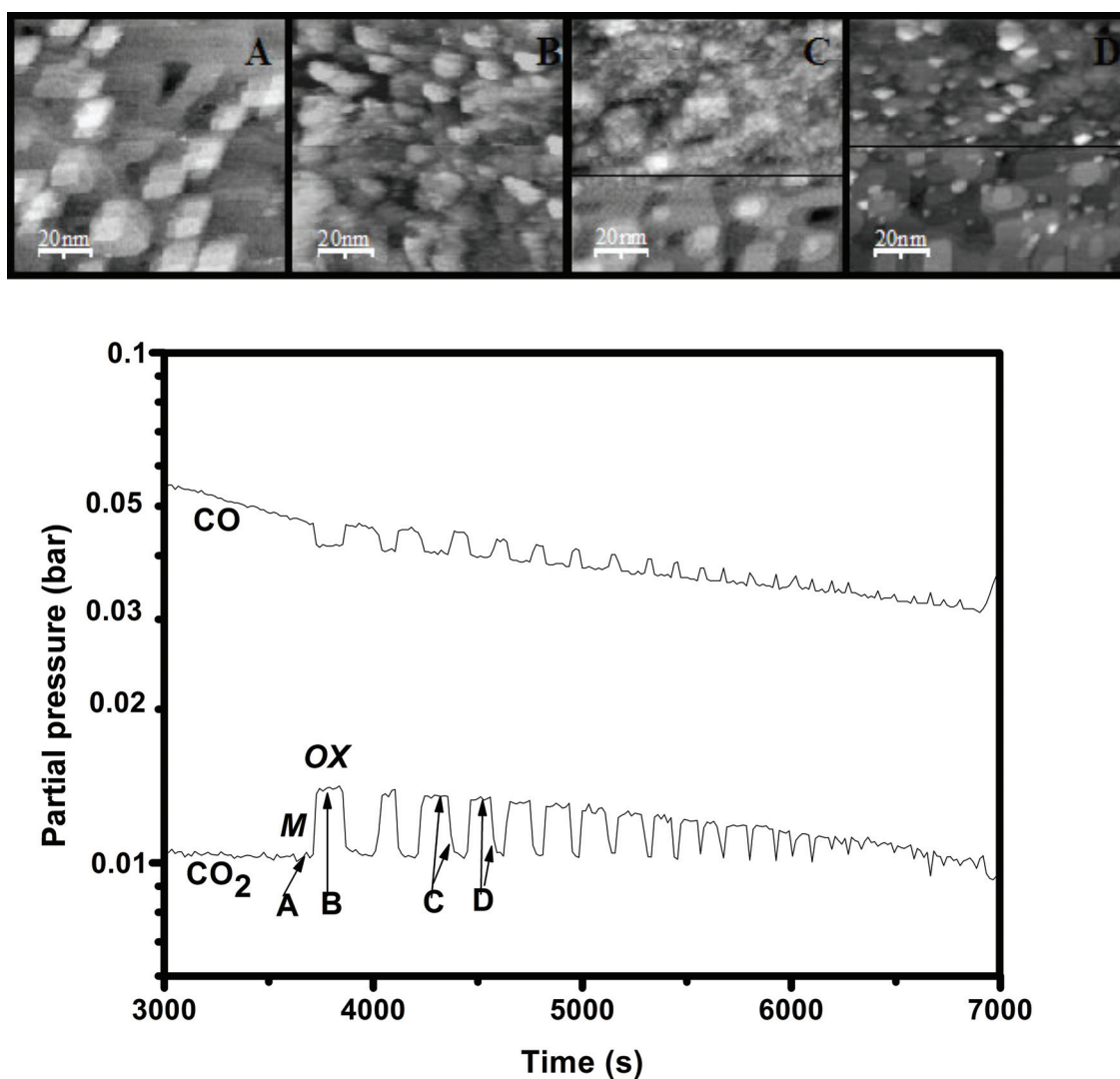
Figure 3.3 STM images (upper part; 100 nm × 100 nm) simultaneously recorded with the kinetics of the reaction (lower panel) under oscillation conditions. Letters A-D in the lower panel indicates the time at which the images have been taken. The letter M from the kinetics graph stands for the metallic surface, while Ox corresponds to the oxidic surface. The tunnelling conditions were: $V_t = 100$ mV, $I_t = 0.2$ nA.

The acquisition of the STM images under reaction conditions where the oscillations occurred has been very difficult. The CO oxidation reaction is highly exothermic. The switching in the reactivity was accompanied by small changes in sample temperature, reflected in the thermal drift visible in the images. Due to the repeated phase transitions between the oxide and the metal the surface diffusion made the tip unstable.

Figure 3.4 displays oscillations in the reaction rate during CO oxidation over Pd(100), acquired at a constant total pressure of 1.25 bar and three different temperatures. In Fig.3.4 a two series of oscillations can be seen at 408 K. Figure 3.4 b shows two periods from the second series. The oscillations are regular and their shape is almost identical. The oscillations in Fig .3.4 c and d were acquired at 413 K and 403 K respectively. The shape and the period of the oscillations vary upon the variation in the temperature as illustrated in fig. 3.4.

(a) (b)

(c) (d)
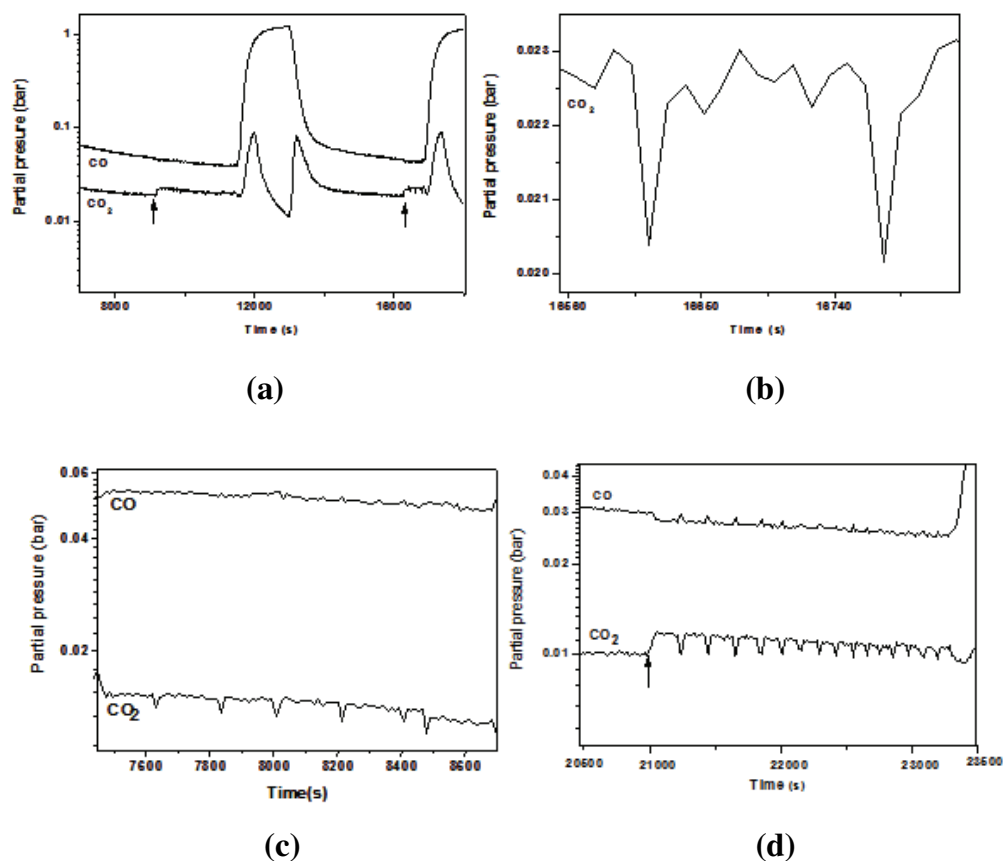
Figure 3.4: *Oscillatory behaviour of CO oxidation over Pd(100) at a total pressure of 1.25 bar and temperatures of (a) 408 K, (b) 408 K, (c) 413 K and (d) 403 K.*

26

3.6 Summary for CO oxidation on Pd(100)

Oxidation of CO on a Pd(100) surface has been studied at atmospheric pressure and various temperatures around 410 K. Under these reaction conditions the reaction rate exhibits bistability, hysteresis and oscillations. The traditional Langmuir-Hinshelwood reaction runs on the metallic form of the palladium surface. At high partial pressures of O_2 the palladium forms a surface oxide, which introduces a Mars-van-Krevelen reaction mechanism and is the most active form of this model catalyst. Our experimental results show that it is essential for the hysteresis in a P_{CO_2}-versus-P_{CO} plot to be counter-clockwise for spontaneous reaction oscillations to occur.

In combination with these "in situ" STM experiments, we have also performed "in-situ" surface X-ray diffraction measurements at the European Synchrotron Radiation Facility (ESRF) in Grenoble which have confirmed the formation of a surface oxide on Pd(100) under similar reaction conditions and have resolved its atomic-scale structure. The X-ray results show that the oxide is typically 1.5-3 nm thick and slowly grows in time and that the structure is that of nearly completely relaxed PdO(001) oriented with its c axis parallel to the [011] axis of the Pd substrate [29]. Another important observation made with by both techniques, STM and SXRD, is that during the reaction on the oxide the surface continuously roughens due to the Mars van Krevelen mechanism. When the reaction rate oscillated, the Pd(100) surface was observed to periodically evolve back and forth between a smoother and a rougher morphology, roughness building up on the oxide surface and reducing again on the metal surface. In the next chapter, we will use this observation of variations in surface roughness as the basis for a new feedback mechanism, which we propose to be responsible for the oscillations between a smoothening, low-reactivity metallic surface and a roughening, surface oxide with higher reactivity.

Having investigated the oxidation of CO on the low-index (100) surface of Pd, we turn to CO oxidation on high-index surfaces in the next section.

3.7 CO oxidation over high-Miller-index palladium surfaces

3.7.1 Motivation

It is well known that industrial catalysts are not perfectly flat, low-Miller-index single crystal surfaces. The investigation of chemical reactions on surfaces with different types of intrinsic defects, such as steps, kinks, vacancies or adatoms, represents an important step to overcome the materials gap between traditional academic studies and industrial 'reality'. There is ample evidence in the literature that defects such as steps play a significant role in many reactions at the solid-gas and solid-fluid interfaces,

for example by acting as the preferred adsorption sites for reactant molecules. The morphology of a surface plays an important role not only in processes related to heterogeneous catalysis, but also in other physical and chemical phenomena, e.g. involving the stability of crystal shapes and the diffusion dynamics of a crystal, film growth, corrosion, etc. Due to their special structural and electronic properties the so-called vicinal or stepped surfaces are the perfect candidates for investigations of these effects. A short introduction to the subject is given in the next pages, followed by a detailed description of our experimental results concerning CO oxidation over two different vicinal palladium surfaces.

3.7.2 Vicinal surfaces - an introduction

A crystal surface cut at a small angle with respect to a high-symmetry plane [h k l] is called a vicinal surface. Such a 'miscut' surface consists of terraces of the high-symmetry plane, separated by parallel atomic steps running across the sample in a direction dictated by the cut. Therefore, vicinal surfaces are also known as stepped surfaces [30-31]. Due to their structure vicinal surfaces introduce additional properties compared with flat surfaces [32]. The structure around a step atom is different from that of around a terrace atom, simply because of the reduced number of neighbours (lower coordination number). Step atoms generally relax further away from regular lattice positions than terrace atoms. There are two reasons for this. Usually the entire surface is under stress [33], often tensile, and at the steps the atoms can respond to this stress by translating over a small fraction of lattice spacing. But also at an unstressed surface there are relaxations. One of the primary causes for this is that the electrons of the solid react to the presence of the step and attempt to minimize the energy of the defect by spreading out in a way that makes the discontinuity at the step less abrupt. This so-called Smoluchowski smoothing [34] generates an electrical dipole moment, which, in turn, makes the step atoms shift. Since the electronic structure of the steps differs from that of terraces, one may expect their chemical reactivity to be different as well. In particular, in view of the reduced coordination of the step atoms, step sites often provide extra strong binding to adsorbates. Steps are the locations where crystals tend to grow and where adsorbates tend to accumulate. One should keep in mind that the upper and lower sides of a step are different. This is illustrated by the so-called Erlich-Schwoebel effect (ESe), which describes the asymmetry between the diffusion barriers for atoms to attach to a step when they approach from the upper and from the lower terrace [35-36]. Often, vicinal surfaces do not have a completely regular array of steps and kinks. Most vicinal surfaces undergo a roughening transition already below room temperature, which introduces randomness in the distribution of step and kink distances and introduces extra, i.e. 'unnecessary' kinks [37]. From the perspective of crystal growth, vicinal surfaces are known to suffer from two types of

instabilities, step bunching and meandering, which may arise either as a consequence of step-step interactions or by high step energy [38]. Bales and Zangwill first pointed out the meandering instability in 1990 [39], which is the phenomenon that the steps are morphologically unstable during growth in the presence of an ESe (i.e. when it is more difficult for atoms to attach to the step from the upper terrace). The instability is due to the fact that the step velocity of the growing surface will be larger in regions of positive step curvature due to the geometrical increase of the adatom capture zone. A second form of transport-driven morphology change has been observed in 1989 by Lathyshev *et al.* [40], who showed that electromigration leads to step bunching on Si(111) vicinal surfaces. To simplify the step bunching process can be attained by the means of changing the temperature (a thermodynamically field) or chemical potential (due to the adsorption of molecules on the surface).

In the presence of adsorbates stepped surface often undergo structural phase transitions, e.g. faceting. For example, in the presence of oxygen, Ni(977), Pt(554), Rh(775), Rh(332) and other vicinal surfaces show a reversible doubling of the average terrace width and step height [41-44].

In order to address the effect of steps, we have investigated two vicinal palladium surfaces, one vicinal to a (100) orientation, namely Pd(1.1.17), and the other with a vicinal to the (111) orientation, namely Pd(553). In both cases the steps are close-packed, i.e. they run along a [110]-direction, or, equivalently, they can be viewed as one atom wide (111)-type terraces. In the remainder of this chapter we show the behavior of these two surfaces under the conditions of high-pressure CO oxidation.

3.7.3 CO oxidation over Pd(1.1.17)

Interaction of CO and O_2 with the stepped Pd(1.1.17)

The left panel of Figure 3.5 shows the starting point of our experiment on Pd(1.1.17). After cleaning the surface by repeated cycles of Ar ion bombardment and annealing, similar to the recipe for Pd(100), we imaged the surface with the Reactor-STM. Although the vacuum in the Reactor-STM is rather poor, we observe a pattern of narrow terraces and steps, with the average terrace width of 2.05 nm and the 0.22 nm step height corresponding to the expected structure of the clean Pd(1.1.17) surface at room temperature. The right panel of Fig.3.5 shows the effect of exposing this surface for 2 h to 1.25 bar of CO at a temperature of 420 K. The STM image shows an increase in the average terrace width by a factor of 2.

Also exposure to oxygen had a major impact on the vicinal Pd(1.1.17) surface. Figure 3.6 shows the surface in an oxygen rich flow at 413 K, after having been pre-exposed to CO. We observe terraces with 4 to 5 times the width of terraces on clean Pd(1.1.17) and a substantial density of kinks. Of

course, the step heights have increased by the same factor as can be seen from the two height profiles in Fig.3.6. Although we have not performed a separate experiment where the surface was first freshly prepared in UHV and then exposed to pure O_2, we assume that the structure in Fig.3.6 reflects the equilibrium structure of the vicinal surface in the oxygen (or, more accurately, oxygen-rich)atmosphere.

Initial Structure   **Double Structure**
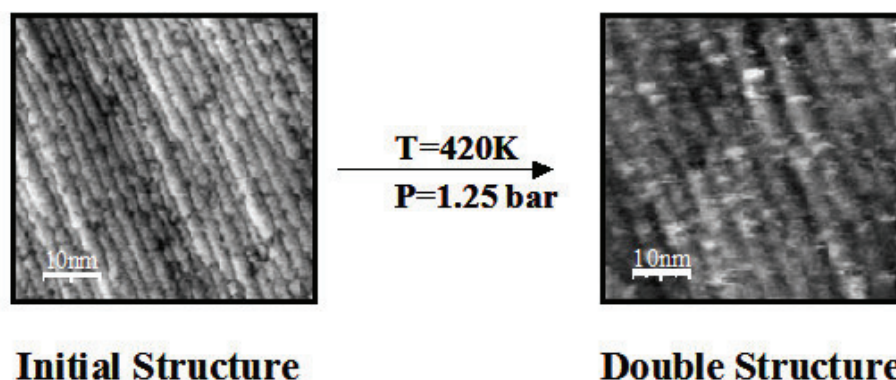
Figure 3.5: Doubling of Pd(1.1.17) terrace width due to exposure of the surface to CO. Left panel: starting surface at room temperature in (poor) vacuum (10^{-2} mbar). Right panel: surface after 2 h at 420 K in 1.25 bar of CO. Both images measure 50 nm × 50 nm. V_t=0.4 V, I_t=0.2 nA.
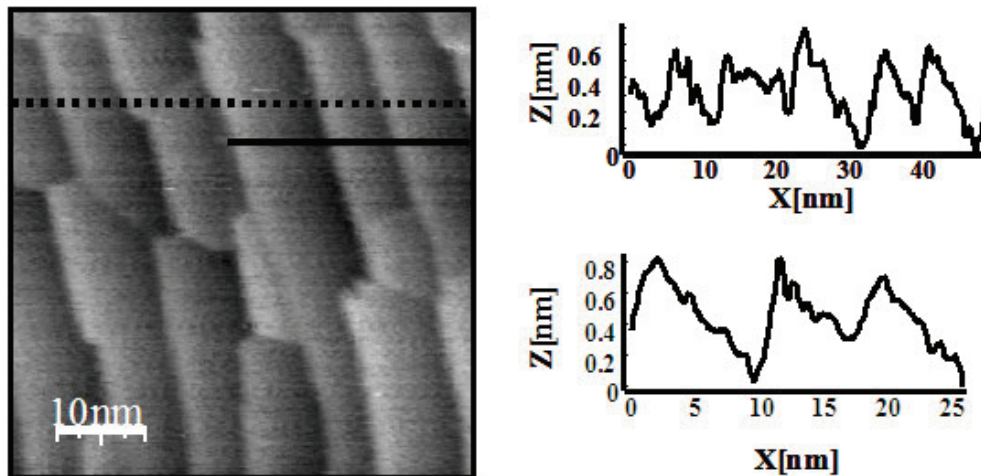
Figure 3.6: Pd(1.1.17) after a single oxidation-reaction cycle at total pressure of 1.25bar and 413K. The average terrace width is between 4 and 5 times the equilibrium terrace width on the clean surface. The two height profiles run along the dotted and continuous lines in the STM image (50 nm x 50 nm) and illustrate the changes in the terrace width and height.

This notion is further substantiated by the observation that each of the subsequent reduction-oxidation cycles of CO- and O_2-exposure returned the surface to the same structure. The single-terrace-width structure of clean Pd(1.1.17) was recovered only after repeated cycles of sputtering and annealing in UHV. The double-terrace-width structure was obtained only after exposing a freshly prepared surface to pure CO.

Oxidation-reduction process

Figure 3.7 shows a combination of the partial pressures of the reactant gases CO and O_2 and the reaction product CO_2 measured during one reduction–oxidation cycle and a selection of simultaneously recorded STM images. In the upper panel of the Figure 3.7 the reaction kinetics is depicted. At $t = 0$ s we changed the composition of the gas mixture from CO-rich to O_2-rich. In response, the reaction rate, which is again reflected in the measured CO_2 partial pressure, passed through a maximum at $t = 208$ s, similar to the reaction kinetics of CO oxidation on Pd(100) described in the first part of this chapter. This behavior is consistent with the Langmuir–Hinshelwood mechanism of competing adsorption by CO molecules and O atoms with a maximum reaction rate under conditions of equal coverages of reactants ($\theta_{CO} = \theta_O = 0.5$). After the maximum at $t = 208$ s the reaction rate monotonically decreased in time, following the decrease in CO partial pressure. At $t = 4867$ s (indicated by the arrow in Figure 3.7) the reaction rate suddenly increased by a factor 1.6. Simultaneously with this increase in the CO_2 signal, the mass spectrometer recorded an equally large decrease in the CO partial pressure.

The changes in reaction rate and kinetics strongly suggest that the surface was oxidized and that the reaction switched to the more efficient Mars-van-Krevelen mechanism. The catalytic system maintained its higher reactivity until $t = 5733$s, at which point we increased the CO partial pressure. This led to an immediate downward step in the reaction rate consistent with the removal of the surface oxide. After this, the reaction rate increased and passed through a maximum at $t = 6334$ s, corresponding to Langmuir-Hinshelwood kinetics on the metallic surface. After the maximum, the reaction rate dropped as the surface became increasingly poisoned with CO.

The lower panel of figure 3.7 displays a selection of images from the STM movie recorded simultaneously with the kinetics described above. Image A was recorded at $t = 3000$ s, in the oxygen rich flow at low reaction rate. As expected from the kinetics, the image shows the oxygen-covered metallic Pd(1.1.17) surface, containing flat terraces with a 4- to 5-fold increased width, separated by steps with a 4- to 5-fold increased height. Image B was acquired just before the reaction rate suddenly increased. Although the image suffers somewhat from a double tip effect, it shows that

the surface is still in the same state as in image A. Image C was recorded consequently after image B. The step up in CO_2 partial pressure happened during one scan line at the beginning of image C. Interestingly, in image C the steps can still be distinguished, even though there is a definite change in surface morphology (roughening) compared to image B.
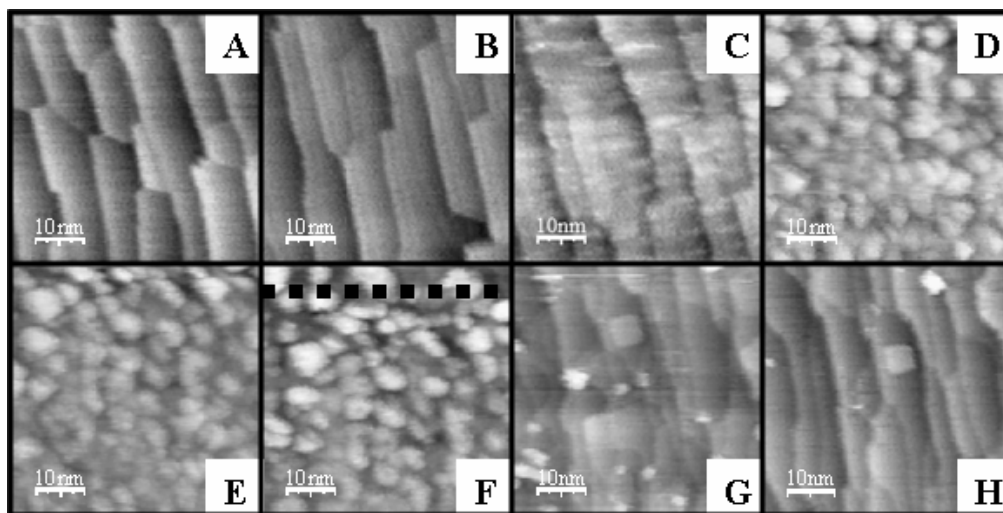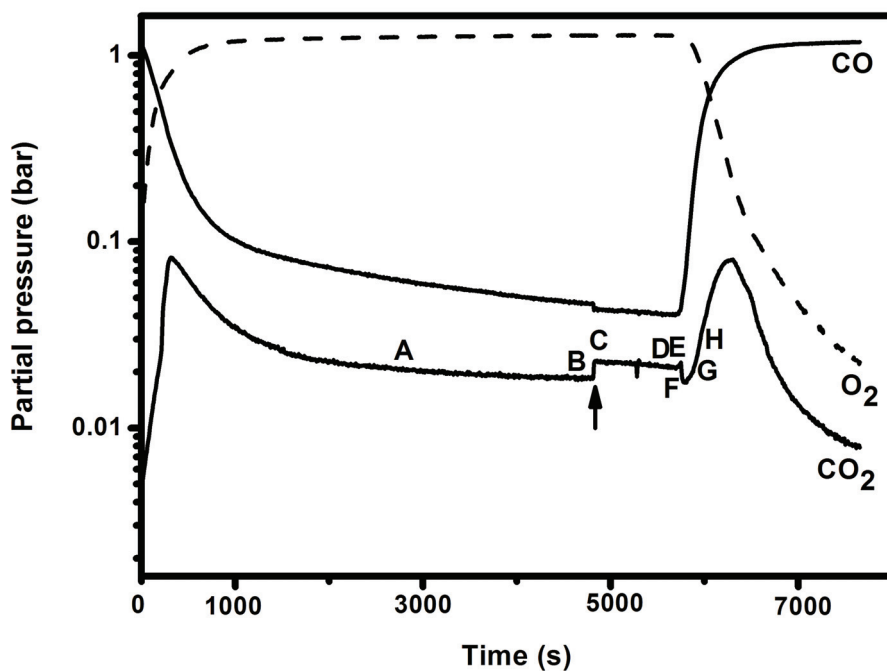
Figure 3.7: STM images and mass spectrometer signals measured simultaneously during a cycle of CO oxidation, from a CO-rich mixture to O_2-rich and back to CO-rich, on the Pd (1.1.17) surface at T=413 K and P_{tot}=1.25 bar.

Images D and E have been acquired after the surface had been kept in the high-reactivity state for approximately 14 minutes. The initial roughness visible in image C has developed into cluster-type structures. Such structures have been observed before and have been referred to as the "cauliflower structure" [45]. We will return to the evolution of this morphology in more detail below.

The changes in the surface structure, correlated with the stepwise increase in the reactivity are very similar to what we have observed in earlier experiments on Pt(110) and Pd(100) under atmospheric pressures of oxygen-rich CO/O_2 mixtures at elevated temperatures [28-29] and confirms our earlier suggestion that also Pd(1.1.17) undergoes a surface phase transition from a metal with a low reactivity to an oxide with higher reactivity. From the statistics of images D and E we obtain a density of 85 ± 10 clusters per image of 50 nm × 50 nm, with a diameter in the range of between 4 ± 2 nm. During image F the reaction rate stepped down. The lower part of the image still shows the surface oxide. The reduction in reaction rate took place at the location of the dotted line, above which a modest change can be observed in the appearance of the surface: the cluster density is lower (the smaller clusters have disappeared) and a few steps are faintly visible. Also, the tip seems to have changed. In the image acquired immediately after this (G), most cluster structures have disappeared, and the structure with terraces and steps, characteristic for the metal surface, is clearly visible. The remaining cluster structures have heights corresponding to multiples of the interlayer distance of Pd(100). The largest island has a square symmetry, reflecting the geometry of the (100) plane of palladium. Due to the coarsening of the adatom islands and their coalescence with the steps, the surface smoothens further, as can be observed by comparing images G and H.

In order to obtain additional information about the surface evolution, we have extracted the step density from the selected images in Fig.3.7. The result is shown in figure 3.8. The step density has been calculated as the sum of all the steps length divided by surface area. As long as the surface is in the metallic state, i.e. from image A to B and after image E, the step density decreases. When the surface is oxidized, between images B and C, the step density is increased suddenly by a factor of 1.6. As long as the surface stays in its oxidic form, the step density slowly increases further. We find that the step density of the metallic surface immediately after the oxide has been removed is higher than that just before the oxide is formed, consistent with the presence of decaying clusters in the first minutes after the oxide is reacted away.
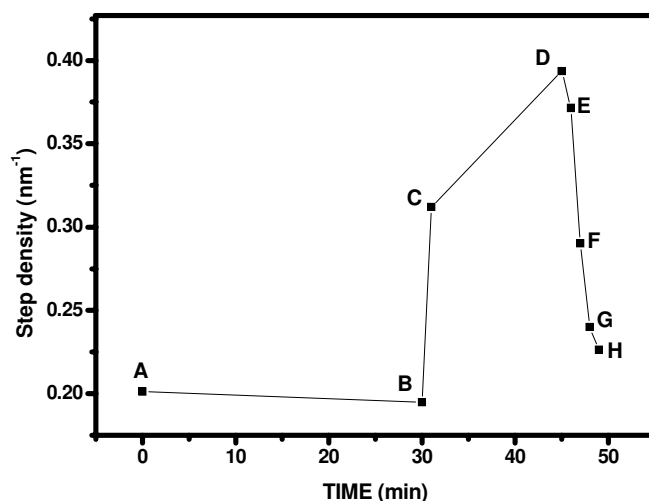
Figure 3.8: *Evolution of the roughness (step density) on the Pd (1.1.17) surface during the reduction-oscillation cycle of Fig. 3.7. The letters indicate the times of the individual STM images shown in Fig. 3.7.*

The oxide evolution in time

As already mentioned above, the initial oxidation of the vicinal surface was responsible for a modest roughening visible in image C in Fig.3.7 (e.g. the bright stripy structures, which developed from the step edges into the terraces). Since image C from Fig. 3.7 was the first image acquired in the high-activity phase we infer that at the beginning of the oxidation process the vicinal metal surface is covered by a thin oxide layer that covers the entire surface and that steps play a role as nucleation centres for the subsequent growth of the oxide clusters that make up the "cauliflower" structure. In order to illustrate this point we display in Figure 3.9 the STM images recorded between image C and an image showing a structure similar to the one in image D. The six images shown below have been acquired consecutively one after one. The recording time for an image was 46 s so image C_5 has been acquired at approximately 6 minutes after image C. As one could see the morphology of the surface changed rapidly due to high O_2 exposure. These images reveal how the (oxide) clusters develop from height variations in the initial thin oxide film (indicated in the image C by ellipses) that appears to originate from the steps and protrude into the terraces. It has been shown by Xu and Yates that for Pt(533) the lowest-energy adsorption site for CO and O_2 is at the step, whereas the highest probability of reaction is between CO molecules adsorbed on the terrace and oxygen atoms adsorbed on a step [46]. If we would replace the oxygen adsorbed on a step with the oxide which forms at the steps, and correlate this with the observation that the oxide has higher reactivity, their theory might ally also for CO oxidation on Pd(1.1.17).
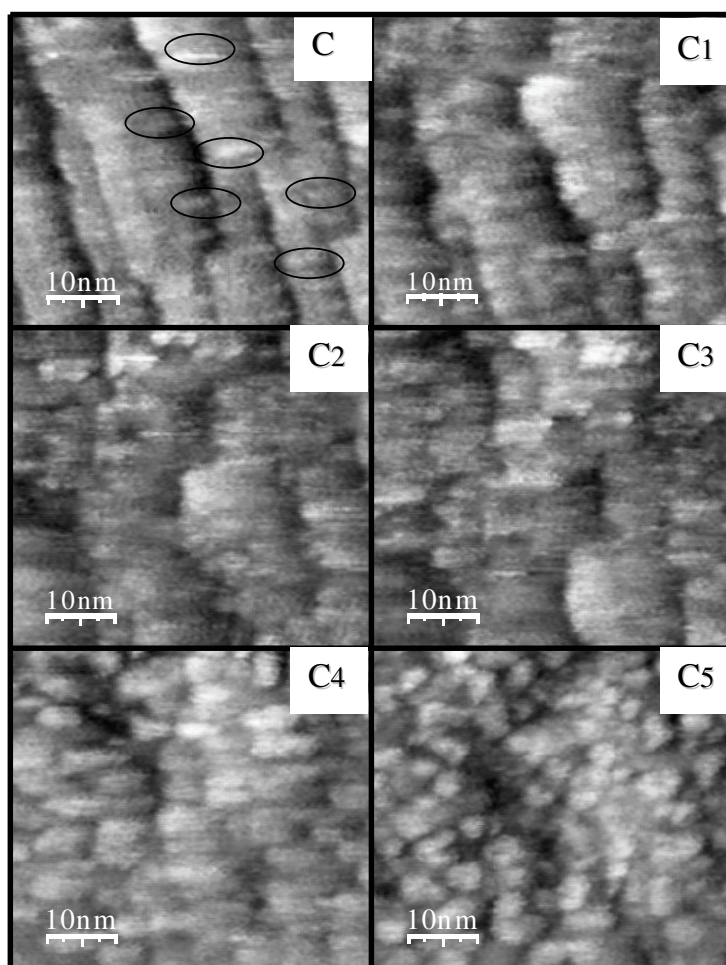
Figure 3.9: STM images (50nmx50nm) illustrating the nucleation and growth of the palladium oxide clusters. At the beginning of image C, the reactivity had already stepped up, indicating that the entire surface had already formed a thin oxide. The sequence of images shows that the initial stages of cluster formation are assisted by the presence of steps.

The development in time and the stability of the palladium surface oxide has been investigated in a different experiment performed at the same pressure of 1.25 bar, but a slightly different temperature of 417 K. Figure 3.10 displays the STM images and the simultaneously recorded reaction rate. Image K has been acquired immediately after the upward step in the reaction rate indicated by arrow 1 in the lower panel. Images K-N show that the oxide clusters structures have an imperfect square shape. Clear vertical lines are also observed within these images. After some time the fine lines disappeared and the number of clusters increased (image O and P). Finally the oxide clusters evolve to a more rounded shape, forming the "cauliflower" structure mentioned above (images R-W).

In order to check the stability of the oxide, we intentionally exposed the oxide surface to short pulses of CO. Image S has been recorded just

before the first CO pulse. Then the valve to the CO bottle has been opened for 10 s. Image T has been recorded during the first increase in the reaction rate marked by the arrow 2. The surface shows very similar oxide clusters to those in image S. Images U and V have been acquired during the second and third CO pulses respectively, indicated in the figure by arrows 3 and 4. Although there is some loss of resolution in these images, due probably to a change in the tip, the morphology of the surface seems to have remained largely unchanged.

The reaction rate exhibits downward spikes during the increases in CO_2 production. We will show later in this manuscript that the spikes are in fact oscillations. Similar to the case of Pd(100), the vicinal surface switches spontaneously between its metallic state and the surface oxide. The time spent in the metallic phase is too short compared to our scanning speed to show up clearly in the STM images. For this reason we are able to see only the oxidic phase.
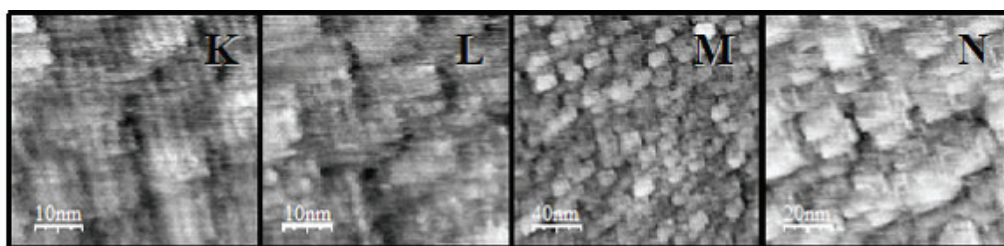
| t=0 min | t=5 min | t=11 min | t=21 min |

| t=26 min | t= 32 min | t= 50 min | t=90 min |

| t=104 min | t=115 min | t=137 min | t=161 min |
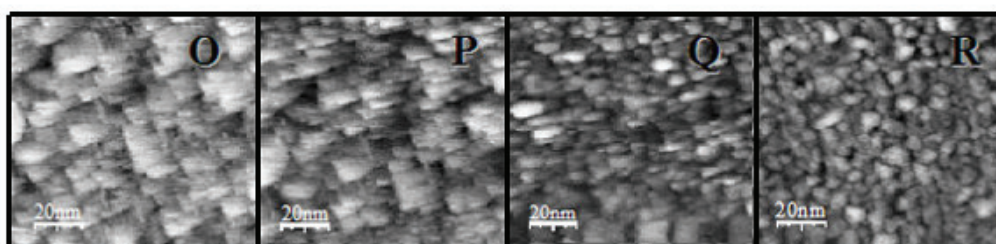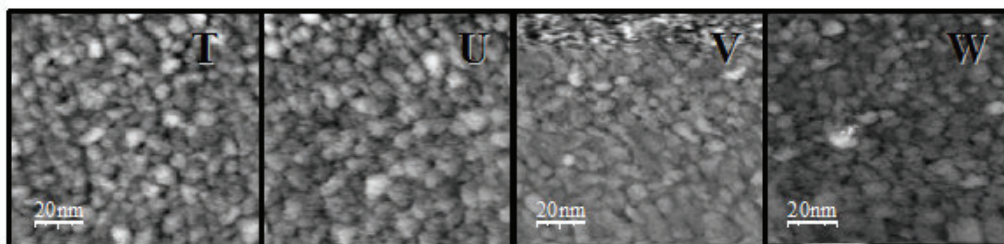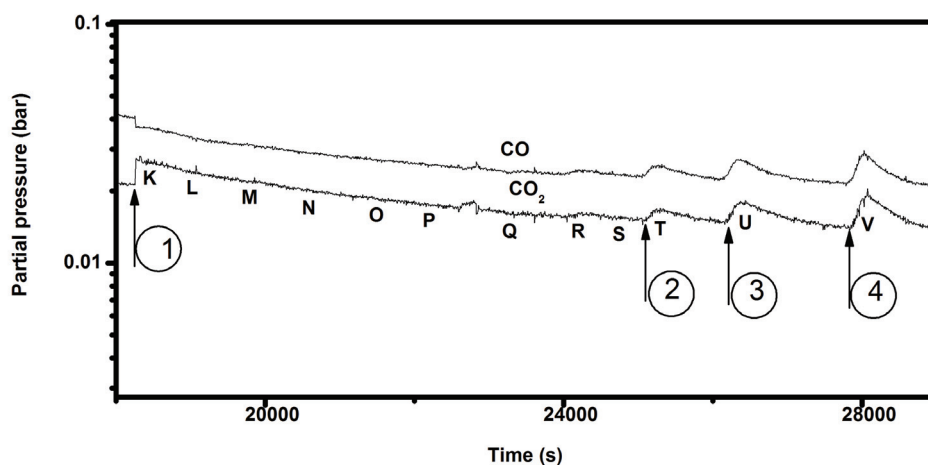
Figure 3.10: *STM images and simultaneously recorded reaction rate on Pd(1.1.17) at P_{tot} =1.25 bar and T = 417 K. Arrow 1 indicates the spontaneous upward step in reactivity that is associated with the formation of the surface oxide. Arrows 2, 3 and 4 mark the times where the CO pressure was manually increased to 0.025 ,0.027 and 0.029 bar for a short duration of 10, 15 and 30 s. the size of the STM images is 50nm×50nm (K-L),200nm×200nm (M) and 100nm×100nm (N-W). V_t=1 V and It=0.2 nA.*

Oscillations and kinetics

If we plot the partial pressure of CO_2 as a function of the CO partial pressure, while the partial pressure of O_2 is kept constant, all the data from the experiment described above fall on two branches, as seen in figure 3.11. This is similar to what has been observed on the other surfaces introduced in this thesis. One branch corresponds to the oxidic surface with higher catalytic activity. The other branch corresponds to the metallic surface, with lower reactivity. For this particular experiment the catalytic system exhibits bistability and the system oscillates between an oxide and a metallic surface covered with an oxygen-dominated mixed overlayer of CO molecules and O atoms. In contrast to Pd(100) the oscillations on the vicinal surface do not have the square waveform shape and their period is very short. Experiments performed at a constant total pressure of 0.5 bar showed the same behaviour, with the data separating again in two branches.

At a total pressure of p = 1.25 bar the surface switched from the metal to the oxide (high reactivity) at a ratio Pco/√Po$_2$ equal to 0.034 √bar. The phase transition back to the metal happened at a ratio equal to equal to 0.030 √bar. For the lower pressure of 0.5 bar the surface switched to the higher catalytic activity branch at higher ratio Pco/√Po$_2$=0.038 √bar, while the switching back to the lower catalytic activity branch took place a ratio Pco/√Po$_2$ equal to 0.036 √bar.

37
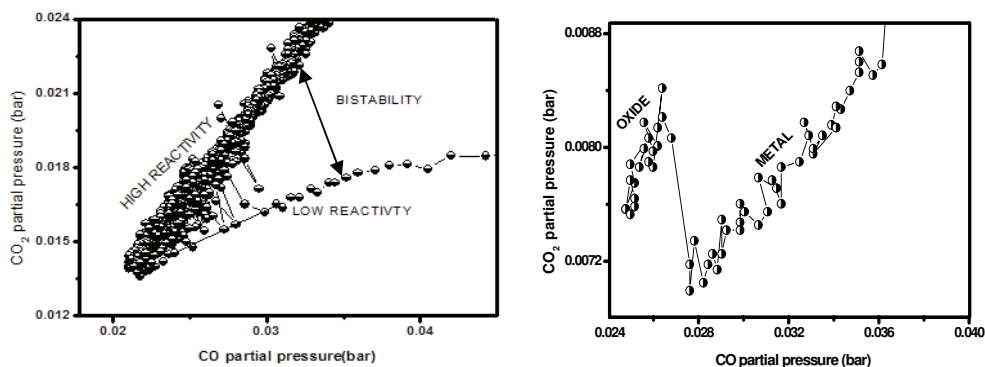
Figure 3.11: Partial pressure of CO_2 (reaction rate) as a function of the CO partial pressure at a constant O_2 partial pressure of 1.25 bar (left panel) and 0.5 bar (right panel) at a temperature of T = 417 K. In both cases we observe two separate branches that we identify as the low-reactivity metallic surface, covered by an oxygen-dominated mixture of CO and O_2, and the high-reactivity oxide surface. The line connects the data points in the order in which they have been measured. The lines that cross over, back and forth, between the two branches indicate spontaneous reaction rate oscillations.

Both data sets show in the CO_2 production rate (upon variation of P_{CO}) a hysteresis with a counter clock-wise (ccw) orientation. As explained previously in this chapter for Pd(100), the ccw hysteresis means that the oxide on Pd(1.1.17) was formed at higher P_{CO} value compared to the partial pressure of CO at which the oxide was reduced again. The ccw orientation of the hysteresis satisfies an important requirement for the existence of spontaneous reaction oscillations [47].

3.7.4 CO oxidation on Pd(553)

In Fig. 3.12 we show the usual combination of the time evolution of the three partial pressures of CO, O_2 and CO_2 and a series of selected STM images obtained during this evolution. The experiment was performed at a constant total pressure of 1.25 bar and a temperature of 410 K. At the beginning of the time sequence in Fig. 3.12 we switched from a CO-rich flow to an O_2-rich flow and at the end we switched back to a CO-rich flow. In both cases we see the rate of CO_2 production go through a maximum, corresponding to the behavior expected for the Langmuir-Hinshelwood reaction on a metallic palladium surface and similar to our observations on Pd(100) and Pd(1.1.17). While in the oxygen-rich flow the catalytic system switched two times to a higher reactivity; first at t = 5061 s for a short time interval (indicated by arrow 1), and a second time at t = 6114 s for a longer period (arrow 2). In both cases simultaneously with the increase in the reaction rate we notice a decrease in CO partial pressure. The critical values

for the CO partial pressures at which the catalyst switched to the higher reactivity were 28 mbar for the first increase and 26 mbar for the second. In analogy with our observations on Pd(100) and Pd(1.1.17), we associate the reactivity changes with the formation of an oxide on the palladium surface.

Image A in Figure 3.12 and the first part of image B (below the dashed line) are characteristic for the metallic Pd(553) surface. The dashed line in image B marks the point in time where the partial pressure of CO_2 stepped up the first time. In the upper part of image B and in image C, which was measured directly after B and corresponds to the maximum in the reaction rate, we observe a clear roughening of the surface, as we have observed also on the other surface orientations of Pd during CO oxidation on the oxide phase of the surface. Image D was recorded immediately after the step down in the reaction rate, and it shows again the morphology of the metal surface. Due to the fact that the density of steps is very high on the (553) surface the oxide cannot become very rough and that the metal returns to its equilibrium smooth state very quickly. Images E-J in Fig. 3.12 show the sequence of surface morphologies recorded on Pd(553) just before and after the second switch to the higher reactivity.
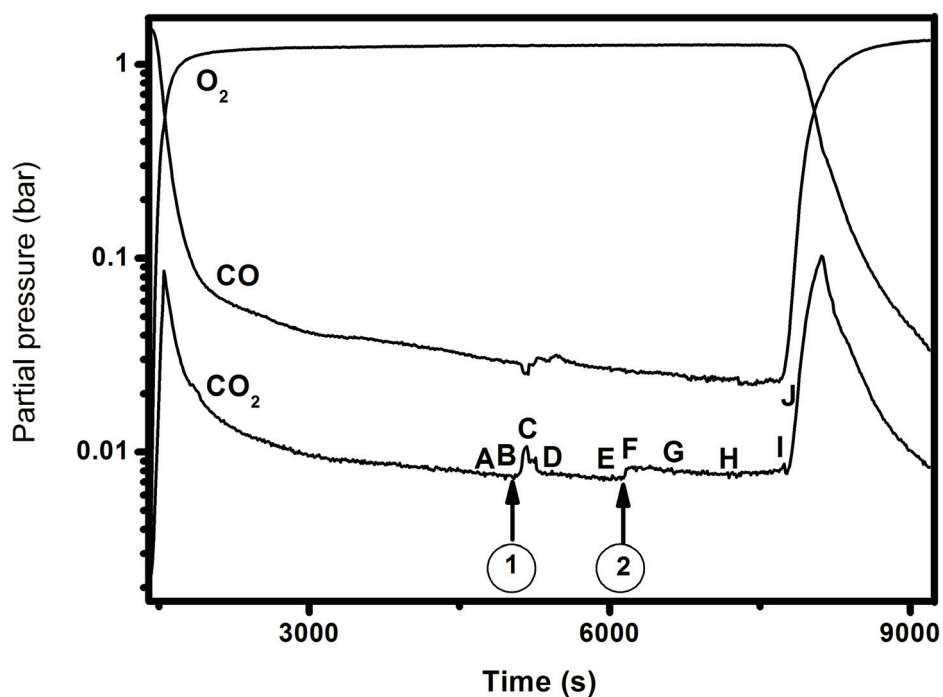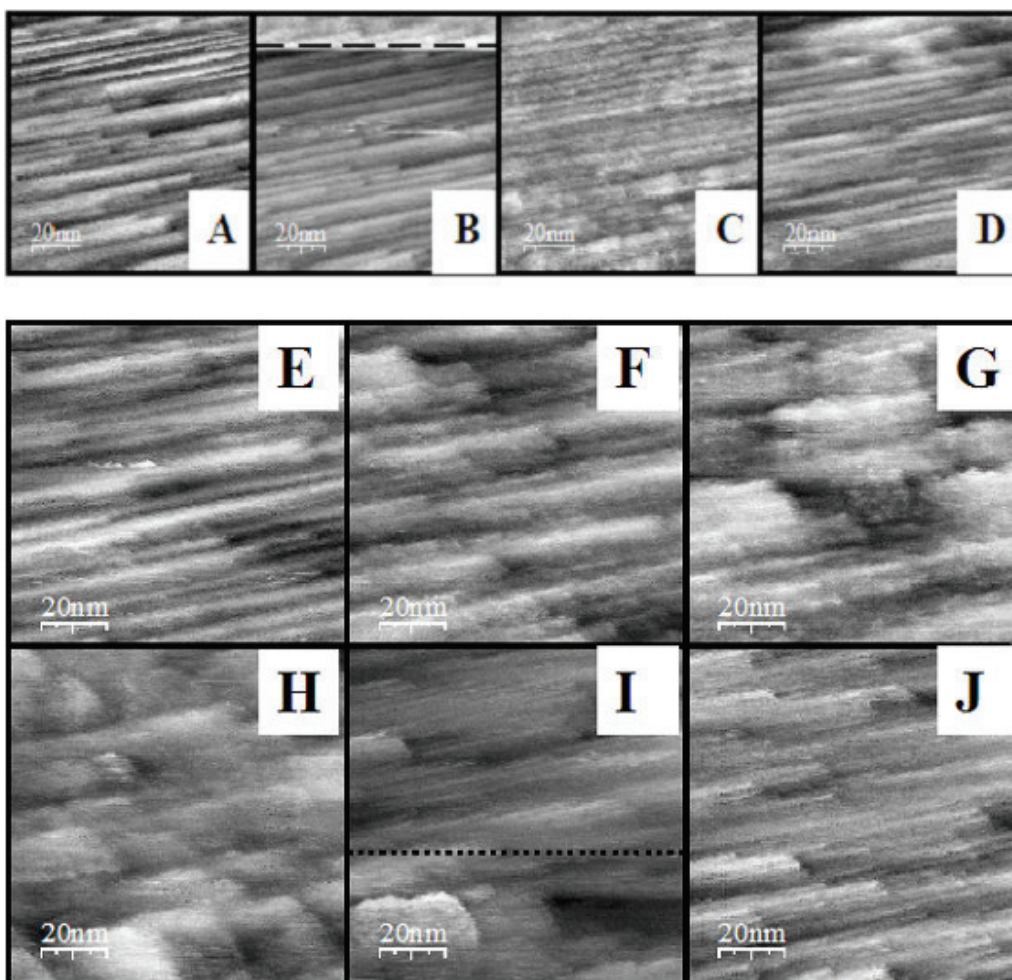
Figure 3.12: *Partial pressures of CO, O2 and CO$_2$ and STM images(100nm×100nm) measured during CO oxidation and a total pressure of 1.25 bar and a temperature of 410 K on Pd(553), while the gas mixture was cycled from a CO-rich mixture to an O$_2$-rich mixture and vice versa. V_t= 0.1V and I_t=0.2 nA.*

Image E shows the metallic surface. The recording of image F took place after the reactivity stepped up (arrow 2 in top panel Fig. 3.12). Images F, G and H show a modest increase in roughness with time. The oxide features evolved from small protrusions to larger cluster-type structures, similar to the development of the oxide on Pd(1.1.17). The upper part of image I and the subsequent image J describe the appearance of the surface after the oxide had been reduced, due to the increase in CO partial pressure. This time, we do not observe any formation of adatom and vacancy islands, after the removal of the oxide. It is plausible that such roughness has been present after the removal of the oxide but that the timescale for the removal of this roughness is very short on the (553) surface as a consequence of the small terrace width.

40

3.8 Conclusions

We have investigated the "in situ" the CO oxidation at ambient pressures and elevated temperatures over two high Miller indexes surfaces of palladium. Pd(1.1.17) is vicinal to the (100) orientation, while Pd(553) is vicinal to the (111) single surface. Both surfaces revealed the formation of an oxide in oxygen rich flow. The oxide has higher reactivity compared to the metallic surface. On the oxide the reaction follows the Mars van Krevelen mechanism, while on the metallic surface it follows the Langmuir-Hinshelwood mechanism. Spontaneously oscillations in the reaction rate have been observed for CO oxidation over Pd(1.1.17). Similar to Pd(100) the oscillations can be interpreted as phase transition between a smooth and a rough surface. No oscillatory behaviour has been observed for Pd(553)

3.9 Reference:

[1]   http://www.stillwaterpalladium.com

[2]   http://education.jlab.org

[3]   S. M. Vesecky, D. R. Rainer, D.W.Goodman, *J. Vac. Sci. Technol. A* **14** (1996) 1457.

[4]   M. Lyubovsky, L. D. Pfefferle, *Appl. Catal. A Gen.* **173**(1998) 107.

[5]   M. Lyubovsky, L. D. Pfefferle, *Catal. Today* **47** (1999) 29.

[6]   M. Lyubovsky, L. D. Pfefferle, A. Datye. J.Bravo, T. Nelson, *J. Catal.* **187** (1999) 29.

[7]   R. J. Farrauto, M.C. Hobson, T Kenelly, E. M. Waterman, *Appl .Catal. A Gen* **81** (1992) 227.

[8]   S. K. Scott, *Oscillations, waves and chaos in chemical kinetics,* (Oxford University Press, 1994.)

[9]   M. M. Slin'ko and N. I. Jaeger, *Oscillating heterogeneous catalytic systems,* (Elsevier, 1994.)

[10]   P. Gray and S. K. Scott, *Chemical oscillations and instabilities, non-linear kinetics,* (Oxford University Press, 1994).

[11]   G. A. Somorjai, *Introduction to Surface Chemistry and Catalysis* (Wiley,New York,1994).

[12]   M. Boudart, *Adv.Catal.***20**(1996)153.

[13]   B. Hammer, O. H. Nielsen, and J. Nørskov,*Cat.Lett.***46** (1997)31.

[14]   C. R. Henry, C. Chapon, C. Goyhenex and R. Monot, *Surf. Sci.***272** (1992)283.

[15]   Y .Li and J. N. Armor, *Appl. Catal. B* **3**(1994) 275.

[16]   S. Ladas, R.Imbihl, G.Ertl, *Surf. Sci.* **219** (1989) 88.

[17]   M. R. Bassett, R.Imbihl, J.Chem.Phys.93 (1990) 811.

[18]   V. Bondzie, P. Kleban, D.J .Dwyer, *Surf.Sci.***347** (1996).

[19]   V. Bondzie, P.Kleban,D.A.Browne, *J.Vac. Sci.Technol.***A 11** (1993) 1946.

[20]   J.G.Mcgarty, V.L.Wong, Y.F.Chang,*Scr.Metal.Mater.***31** (1994) 115.

[21]   E.H. Voogt, A.J.M.Mens ,O.L.J. Gijzeman, J.W.Geus, *Surf.Sci.***373** (1997) 210.

[22]   G. Zheng, E. I. Altman, *Surf.Sci.***462** (2000) 151.

[23]   G .Zheng, E.I .Altman, *Surf.Sci.***504** (2002) 253.

[24]   K. Reuter and M. Scheffler ,*Appl. Phys.A* **78**,(2004)793.

[25]   www.surf-prep-lab.com

[26]   B. L. M. Hendriksen and J. W. M.Frenken, *Phys. Rev.Lett.***89** (2002) 046101.

[27]   B. L. M. Hendriksen, S. C. Bobaru and J.W.M.Frenken, *Surf.Sci.***552** (2004) 229.

[28]   M.L. D. Ackermann *et al.*, *Phys. Rev. Lett.* **95** (2005) 255505.

[29]   M. L. D Ackermann *et al.*, to be published

[30]   B.Lang, R.W. Joyner and G.A.Somorjai, *Surf.Sci.***30** (1972) 440.

[31]   C. Barreteau, F. Raouafi, M. C. Desjonqueres, and D. Spanjaard J.*Phys.:Condens.Matter* **15** (2003) S3171.

[32]   H. C. Jeong and E. D. Williams,*Surf. Sci.Rep.***34** (1999) 1971.

[33]   H. Ibach and W. Schmickler, *Surf.Sci.***573** (2004) 24.

[34]   R. Smoluchowski, *Phys.Rev.***60** (1941) 661.

[35]   G. Ehrilch and F. G. Hudda , *J.Chem.Phys.***44** (1966) 1039.

[36]   R. L. Schwoebel and E. J. Shipsey, *J.Appl.Phys.***37** (1966) 3682.

[37]   M. S. Hoogeman, L. Kuipers, D. C. Schlößer, and J. W. M. Frenken, *Surf. Sci* **447** (2000) 25.

[38] O. Pierre-Louis, G.Danker,, J.Chang ,K. Kassner,C.Misbah, *J.of Cryst.Growth* **275** (2005) 56.

[39] G. S .Bales, A. Zangwill, *Phys.Rev. B* **41** (1990) 5500.

[40] A. V. Latyshev,et al., *Surf.Sci .***213** (1989) 157.

[41] L. Niu, D. D. Koleske, D. J. Gaspar, S. F. King, S .J. Sibener, *Surf.Sci.***356** (1996) 144.

[42] B. Lang, R. W. Joyner and G. A. Somorjai, *Surf.Sci.***30** (1972) 454.

[43] D. G. Castner and G .A. Somorjai, *Surf.Sci.***83** (1979) 60.

[44] G. Hoogers and D. A. King, *Surf. Sci.* **286** (1993) 306.

[45] J. Han, D. Y. Zemlyanov, F. H. Ribeiro, *Surf. Sci.* **600** (2006) 2730.

[46] J. Xu and J. Y. Yates,Jr., *Surf. Sci.***327** (1995) 193.

[47] M. Ehsasi, M. Berdau, A. Karpowicz, K. Christmann and J. H. Block, *New frontiers in catalysis,* Elsevier Science Publishers B.V.,1993.